Proceedings of the ASME 2020
International Mechanical Engineering Congress and Exposition
IMECE2020
November 16-19, 2020, Virtual, Online

IMECE2020-24601

SIMULATION OF ION CURRENT IN OXYFUEL FLAME SUBJECT TO AN ELECTRIC FIELD

Kemu Xu[1],
Virginia Tech
Department of Mechanical Engineering
Blacksburg, VA
kemu@vt.edu

Alexandrina Untaroiu
Virginia Tech
Department of Mechanical Engineering
Blacksburg, VA
alexu@vt.edu

Christopher Martin
Penn State University
Altoona Colege
Altoona, PA
crm28@psu.edu

ABSTRACT

This paper presents a computational model to study ion and electron transportation and current-voltage characteristics inside a methane-oxygen flame. A commercial software is used to develop the model by splitting the simulation into the combustion and electrochemical transportation parts. A laboratory experiment is used to compare the results from the model. The initial and boundary conditions represented in the model are similar to the experimental conditions in the laboratory experiment.

In the combustion part, the general GRI3.0 mechanism plus three additional ionization reactions are applied and results are then used as input into the electrochemical transportation part. A particular inspection line is created to analyze the results of the electrochemical transportation part. Ion, electron number density, and current density are studied along the interval from -40V to 40V electric potential. The ions are heavier and more difficult to move than electrons. The results show that at both torch and work surfaces charged sheaths are formed and cause three different regions of current-voltage relations.

Keywords: Premixed laminar methane-oxygen flame, Ions and electrons distribution, Electric current

NOMENCLATURE

ρ	Density	kg m^{-3}
$\mathbf{v}$	Velocity	m s^{-1}
V	Volume	m^{-3}
t	Time	s
$\mathbf{a}$	Area	m^2
p	Pressure	Pa
$\mathbf{T}$	Viscous stress tensor.	Pa
E	Total energy	kJ
H	Total enthalpy	kJ kg^{-1}
Y_i	Mass fraction of spec. i	
D_i	Diffusivity of spec. i	m^2 s^{-1}
A	Pre-exponential factor	cm,mol,s,K
k	Rate constant	
β	Temperature exponent	
E_a	Activation energy	J mol^{-1}
T	Temperature	K
c_i	Molar conc. of spec. i	kmol m^{-3}
K	Mobility	m^2 V^{-1} s^{-1}
$\mathbf{N}_i$	Number flux	m^{-2} s^{-1}
m_i	Mass of particle i	kg
q	Elementary charge	C
σ_i	Space charge den. of spec. i	C m^{-3}
n_i	Number density of spec. i	m^{-3}
R_u	Gas constant	J mol^{-1} K^{-1}
k_B	Boltzmann's constant	J K^{-1}

[1] Contact author: kemu@vt.edu

1. Introduction

Due to persistent shortcomings in available sensing technologies, mechanized oxyfuel cutting systems have never benefited from the degree of autonomy demonstrated by their competing processes, such as laser, water jet, and plasma cutting. Since typical sensors are highly unreliable in the harsh environment near the high-temperature flame, an alternative method involves finding the co-dependence between critical parameters (standoff, flow rate, F/O ratio, etc.) and the electrical characteristics of the flame. This can be easily measured using a data acquisition unit and power supply.

To understand the relationship between critical parameters and the current-voltage characteristic, the physics of electrons and ions inside the flame needs to be studied. In this paper, a two-dimensional model is proposed to analyze the transport and distribution of electrons and ions. This allows the derivation of the current-voltage characteristic between the torch and work surfaces. To validate the model, a laboratory experiment with a similar geometry arrangement as Martin et al. is used [1]. Recently, a three-dimensional model has been studied for methane-air flame without the work surface [2]. Also, several one-dimensional models have been developed by different researchers [3-5]. Almost all the models are based on a free propagating flame without touching any surface. Two-dimensional models analyze the flame touching a surface under very high voltage and considered only ions as contributing to the current [6]. In our study, a two-dimensional model with methane oxygen flame touching a surface is used to represent an oxyfuel cutting process. Ions and electrons are studied to get the current-voltage characteristics in this process. A two-dimensional model has benefits over a one-dimensional model since it produces important parameters which are difficult to generate in the latter case. Additionally, it requires much less computational time compared to a three-dimensional model.

The main objective of this paper is to present a two-dimensional flame model, which includes the generation and movement of electrons and ions between two absorbing surfaces. The physics of electrons and ions can help illustrate the current-voltage characteristic of the flame. From the model, the electrical characteristic of the flame is analyzed and compared with the laboratory experiment. The commercial software Star CCM+ is used to develop this computational model by splitting the simulations into parts for combustion and electrochemical species transportation.

2. MATERIALS AND METHODS

Since the molar fractions of electrons and ions are very small (maximum is around 10^{-7} in magnitude) in the flow, the velocity and temperature profiles of the flow are assumed to not be affected by the transportation of electrons and ions under a low voltage condition [6]. The whole numerical simulation is split into two parts: a section for combustion and a section for electrochemical species transportation. The combustion part calculates the temperature and velocity profiles of the flow as well as the generation rates of electrons and ions. The model part determining electrochemical species transportation uses the results from the combustion part of the model and calculates the transportation of electrons and ions. This analysis provides the number densities of electrons and ions and the electric potential of the domain. In parallel, the electric current density is illustrated from the electrochemical species transportation and recombination part.

2.1 Geometry

A computational model of the oxyfuel torch was created to replicate an experiment from Martin et al. [1]. Figure 1 shows the experiment setup.

FIGURE 1: Oxyfuel cutting preheating process experiment [1].

The torch, which is made from either copper or steel, is fixed 12mm (.5in) above the work surface. The diameter of the work surface is varied in the laboratory experiment. As present in the laboratory experiment, the preheating process, which is a stable methane-oxygen flame, is analyzed in this paper. Figure 2 shows the simplified two-dimensional CAD domain.

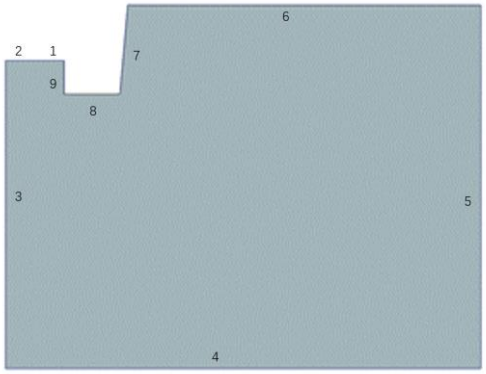

FIGURE 2: Two-dimensional model for the simulation.

To further simplify the two-dimensional model, only half of the physical setup and part of the work surface is considered due to the axial-symmetry of the system. The vertical line of surface 3 represents the symmetry line of the CAD assembly. Together, surfaces 1,2,7,8, and 9 represent the torch tip while surface 1 corresponds to an imaginary annular slot through which the fuel/oxygen mixture is delivered. All other surfaces are prescribed as wall boundary conditions, while surfaces 5 and 6

are set as constant pressure outlets. Surface 3 represents the symmetry plane, while surface 4 represents the work surface. The surface 4 has 0.022m width, and the distance between surface 8 to surface 4 is 0.0127m. The initial conditions are 1 atm pressure, 300K temperature, and composition of standard air. The inlet boundary conditions are selected to correspond to the physical conditions in the experiment, which are 12m/s inlet velocity, 600K inlet temperature, and F/O ratio of 0.833 by volume. A 600K work surface temperature is consistent with conditions during a preheat operation, and matches conditions tested by Martin et al. [7]. The torch surfaces have specified the same fixed temperature of 600K, while the electric potential is varied from -40V to 40 V in 5V increments. The work surface, represented by surface 4 in the figure, has a fixed 600K temperature and 0V. The electrochemical species number densities are 0 at both the torch surface and the work surface because those electrochemical species are absorbed by the metal.

A grid convergence study is performed to select the proper mesh density, resulting in a model with 75,227 grid elements. A much finer model with 1,478,548 number of elements is also analyzed while several flow variables are monitored and compared. Similar velocity, temperature profiles, and number density results are calculated. Thus, the model with approximately 75K cells is selected to save computational time while maintaining the accuracy of the solution.

2.2 Combustion

A premixed laminar methane-oxygen flame is applied in this study. The governing equations of the two-dimensional model are the mass, momentum, energy, and species conservation equations [8].

$$\frac{\partial}{\partial t}\int_V \rho dV + \oint_A \rho \mathbf{v}\cdot da = 0, \quad (1)$$

$$\frac{\partial}{\partial t}\int_V \rho \mathbf{v} dV + \oint_A \rho \mathbf{v}\otimes\mathbf{v}\cdot da = -\oint_A pI\cdot da + \oint_A T\cdot da, \quad (2)$$

$$\frac{\partial}{\partial t}\int_V \rho E dV + \oint_A \rho Y_i \mathbf{v}\cdot da = -\oint_A \acute{q}''\cdot da + \oint_A T\cdot \mathbf{v} da, \quad (3)$$

$$\frac{\partial}{\partial t}\left(\int_{\forall} \rho Y_i\right) d\forall + \oint_A \rho Y_i \mathbf{v}\cdot d\text{a} = \oint_A (\rho D_i \nabla Y_i)\cdot d\text{a}. \quad (4)$$

The reactions of the methane-oxygen flame are combined with GRI 3.0 [9] and three additional ionization reactions from Belhi et al. [10],

$$CH + O \rightleftharpoons CHO^+ + e^-, \quad (R1)$$

$$CHO^+ + H_2O \rightleftharpoons CO + H_3O^+, \quad (R2)$$

$$H_3O^+ + e^- \rightleftharpoons H_2O + H. \quad (R3)$$

Those three ionization reactions are considered the primary reactions to generate charged species in the methane-oxygen flame. The reaction rates are calculated by the Arrhenius' equation, as follows:

$$k = AT^{\beta} exp\left(\frac{-E_a}{R_u T}\right). \quad (5)$$

The coefficient magnitudes of the three additional ionization reactions are listed in Table 1 [3]. The transportation properties are extracted from a methane-air reaction presented by Chen et al. [11].

Table 1: Arrhenius' equation parameters for ionization reactions

Reaction	A	β	E_a
R1	2.512×10^{11}	0.0	7.118×10^{3}
R2	1.0×10^{16}	-0.0897	0.0
R3	1.44×10^{17}	0.0	0.0

Since the species in the combustion simulations can only act as a non-charged species, the electrons and ions are extracted and parsed into the electrochemical species transportation model to complete the analysis.

2.3 Electrochemical species transportation

The electron and ion transportations are analyzed in the second module of the analysis. In the electrochemical species transportation model, a voltage varying from -40V to 40V with a 5V increment is applied to the torch, while the work surface is always grounded. The governing equations [8] of this model are shown below:

$$\frac{\partial}{\partial t}\int_V \rho Y_i dV + \oint_A \rho Y_i \mathbf{v}\cdot da = -\oint_A (N_i m_i)\cdot da + \int_V S_{Y_i} dV, \quad (6)$$

$$N_i = -n_i K_i \nabla\phi - D_i \nabla n_i, \quad (7)$$

$$-\oint_A \varepsilon\nabla\phi\cdot da = \int_V \rho dV. \quad (8)$$

where the source term S_{Yi} is the summation of the generation rate and the recombination rate, while the recombination rate is calculated by equation,

$$\frac{d[E]}{dt} = \frac{d[Ions]}{dt} = -k\cdot[E][Ions]. \quad (9)$$

Transportation of the electrochemical species is consisting of three transport mechanisms: *advection*, *diffusion*, and *migration* as shown in equation 7. The bulk velocity and the temperature profile are imported from the combustion model results.

With the assumption that ions and electrons have a negligible effect on the flow under a low electric potential environment, the results from the combustion model are now considered to be fixed. With these results used as the initial conditions for the electrons and ions transportation model, the generation rate of both ions and electrons are extracted from the combustion model. The mobility of electrons is 0.2 $m^2 V^{-1} s^{-1}$ [2] and 0.0018 $m^2 V^{-1} s^{-1}$ for the ions [12]. The molecular diffusivity is calculated by the Nernst-Einstein relation.

$$D_i = \frac{K_i k_B T}{q}. \quad (10)$$

For the electrical characteristic analysis, since we only have a part of the work surface, the electric current density is calculated by equation [8],

$$J_{ion} = -\sigma_{ion} K \nabla \phi - D \nabla \sigma_{ion} + \sigma_{ion} v, \quad (11)$$

$$J_e = \sigma_e K \nabla \phi - D \nabla \sigma_e + \sigma_e v, \quad (12)$$

$$\sigma_{ion} = q N_A c_{ion}, \quad (13)$$

$$\sigma_e = -q N_A c_e. \quad (14)$$

where the electric current density is related to ion mobility, diffusivity, and bulk velocity. The ion charge density can be calculated based on the molar concentration of ion species.

3. RESULTS AND DISCUSSION

3.1 Premixed laminar methane oxygen flame

The premixed laminar methane-oxygen flame generated in the two-dimensional domain has a triangular flame shape as can be seen in the temperature profile shown in figure 3. The velocity profile and generation rate of electrons and ions are illustrated in figures 4 and 5, respectively.

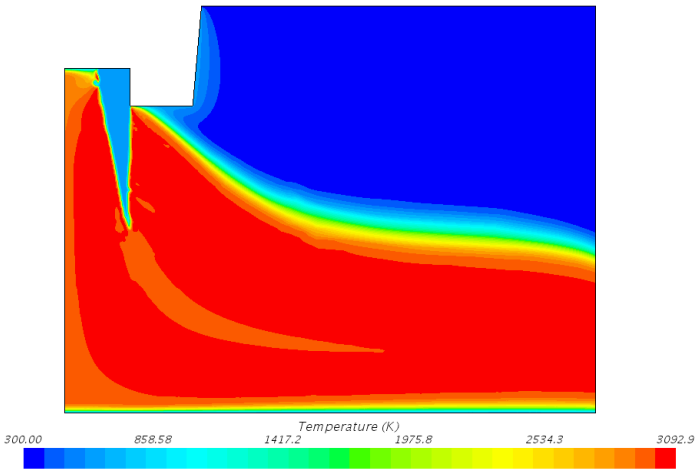

FIGURE 3: Temperature contour plot of premixed laminar methane oxygen flame.

From the temperature profile illustrated in figure 3, one can observe that the temperature is high beneath the V-shape slit, where the diffusivity of electrons and ions is high according to the Nernst-Einstein equation. In the velocity profile in figure 4, the magnitude and direction of the velocity vectors are shown. In a two-dimensional flame, the radial velocity is large in the flow.

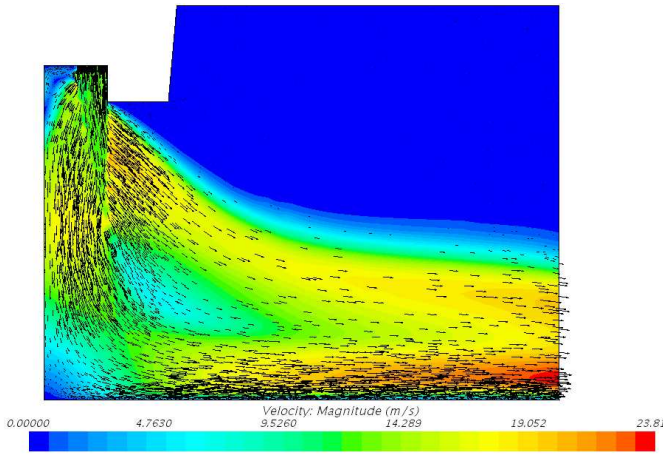

FIGURE 4: Velocity profile of premixed laminar methane oxygen flame.

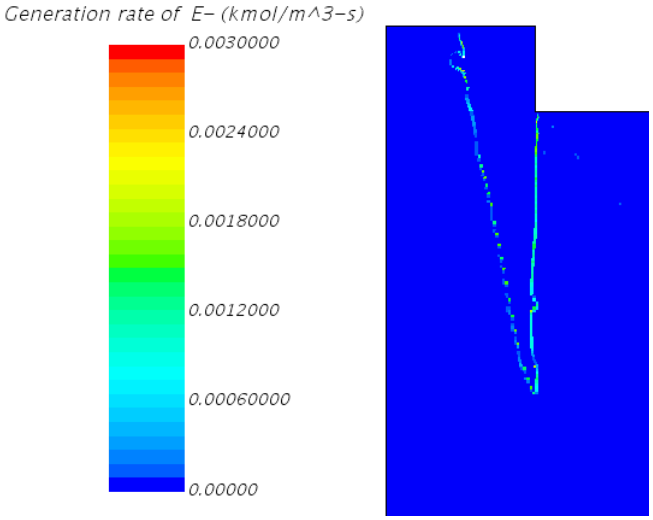

FIGURE 5: Generation rate of electrons in premixed laminar methane-oxygen flame.

On the left side, at the top and bottom corners along the symmetry line, a recirculation region can be seen. In figure 5, the generation rate of electrons is displayed, and the hydronium and formyl cation contain a similar distribution of generation rate as well. Hydronium and formyl cation are the two ions in the ionization reactions. The magnitude of the generation rate for hydronium is close to that of the electrons. Since the magnitude of the generation rate of the formyl cation is substantially less than that of electrons and the hydronium, the formyl cation is neglected to simplify the calculation. Therefore, the ions are essentially the hydronium in the following analysis.

3.2 Electrons and ions distribution

In the electrochemical model, the number density profiles of electrons and ions are resulting from the electrochemical transportation model. The two-dimensional color scheme is

difficult to analyze because the magnitude of the number density changes in a large range.

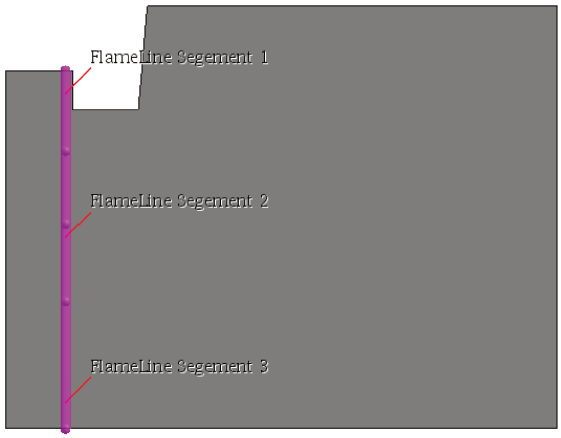

FIGURE 6: Inspection line defined to extract and post-process the results.

Thus, inside the flame area, a virtual line with a 15,000 point resolution extends from the torch surface at the center of the inlet surface in the downward vertical direction. This virtual line is created to extract the results. The flame line has 0.01425m total length. From figure 6, we can see the line is divided into three segments to further analyze and interpret the results. The first and last segment of 0.002 m along the flame line has an increased resolution of 50,000 points because the magnitudes change very rapidly near both surfaces.

Figure 7 shows the number density of electrons and ions along the flame line for the 0V case.

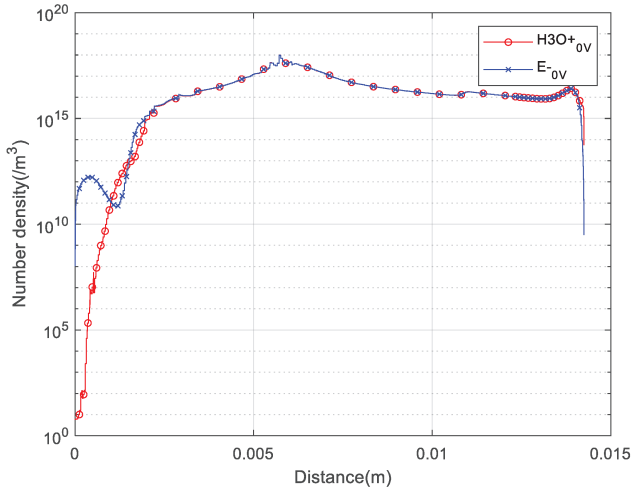

FIGURE 7: Number density of electrons and ions at 0V.

By constraining the torch and work surface's number density to zero using the boundary condition, we can see that saturation comes from the sheath at both surfaces. The flame front is at 0.0057m where both the electrons and ions number density reach maximum. When the torch voltage is 0V, the ions start slowing at the beginning, while the number of electrons increases relatively fast. We find a sudden drop at about 0.0018m. From the geometry, one can see that this location is the position where the torch side ends and a radial velocity appears. The radial velocity leads electrons away. At the workpiece surface, the electrons disappear faster than ions. The number difference between ions and electrons cause the sheaths to form near both upper and bottom surfaces. In the middle of the flame line, the number of electrons and ions are matched. The mass of ions is larger than electrons and the mobility of ions is lower than electrons. This causes the electrons to move more easily than ions. Thus, the electrons tend to move toward the ions because they attract each other and electrons prefer to move.

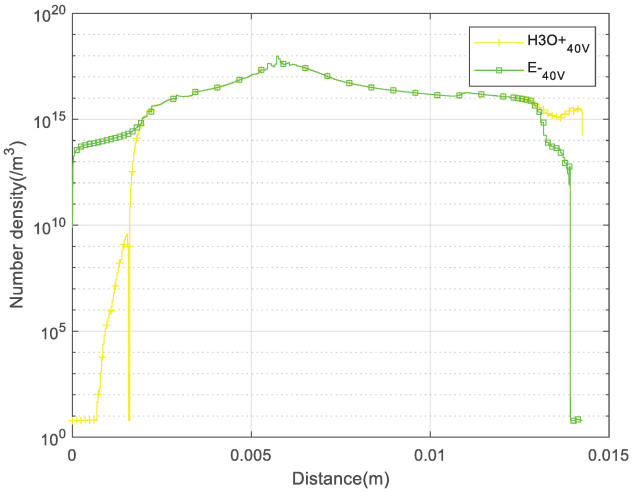

FIGURE 8: Number density of electrons and ions at 40V.

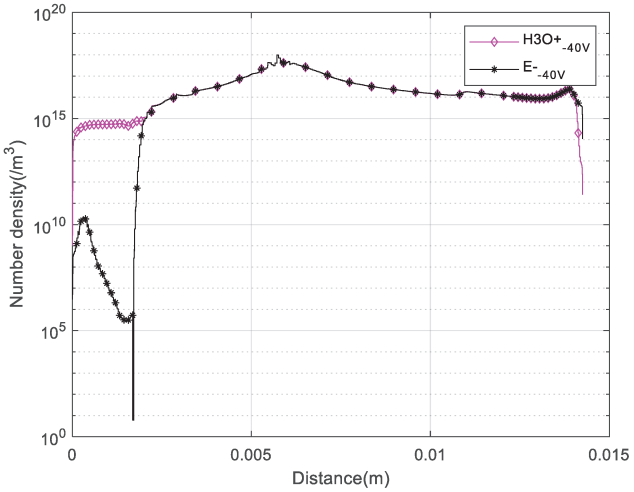

FIGURE 9: Number density of electrons and ions at -40V.

Figure 8 shows the number density of electrons and ions corresponding to the 40V case. From this figure, one can see that when the torch voltage applied is 40V, the number of electrons has increased rapidly at the torch surface and vanished fast at the workpiece surface. Additionally, one can see that the number of ions remains high until very close to the work surface.

Figure 9 shows that when the torch voltage is -40V, the number of ions increases rapidly at the torch surface and

vanishes relatively faster than electrons at the work surface. At the same time, the number of electrons is low at the torch and high at the work surface. The number densities of electrons and ions are shown in figure 10.

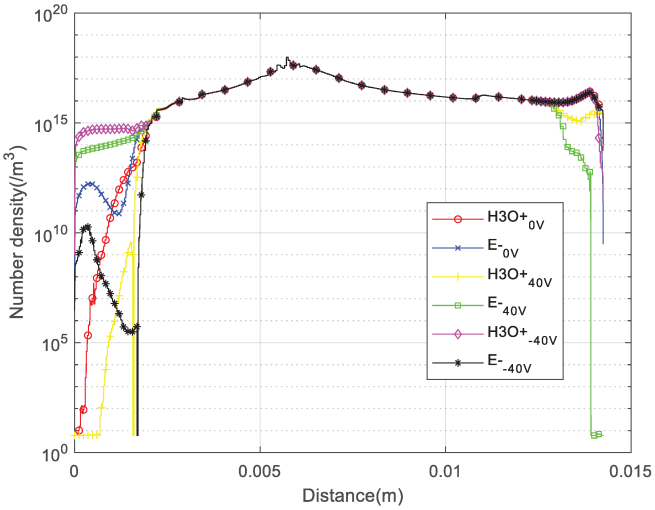

FIGURE 10: Number density of electrons and ions along the center flame line with different voltage.

3.3 Electrical characteristic

Once the number density of electrons and ions have been calculated, the electric potential along the flame line is calculated, as shown in figure 11 for three distinct cases, -40V, 0V, and 40V.

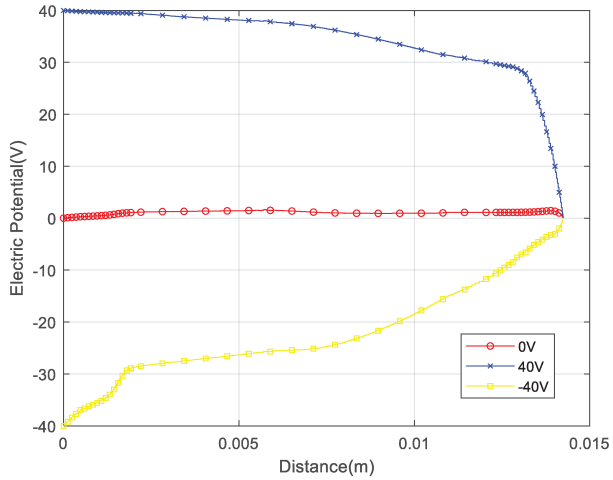

FIGURE 11: Electric potential along the center flame line corresponding to different voltages.

In the 0V case, the plasma potential rises above 0V due to the accumulation of charge in the sheaths. When a strong electric potential is applied, mobile electrons quickly evacuate one of the sheaths, leaving positive charge in their wake and causing one of the sheaths to dominate. In the -40V case, currents are far more substantial, so significant voltage drops can also be seen due to ohmic losses along the flame's length.

Based on all the results from the different torch voltages considered, the electric current density data are extracted downstream of the flame line, which is just above the work surface. The direction of the electric current density is perpendicular to the work surface. The resulting electric current density based on the combination of ions and electrons is shown in Figure 12.

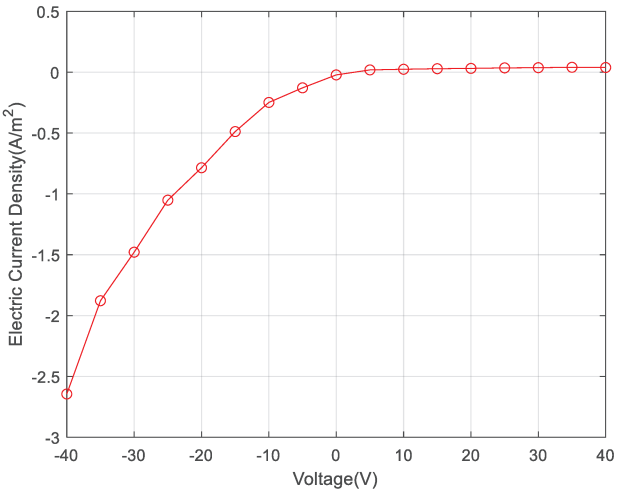

FIGURE 12: Electric current density at the center flame line above work surface with different voltage.

As one can see in the figure, the electric current density changes more rapidly in the negative voltage region. In the positive voltage region, the electric current density increases with increasing voltage, but at a relatively low rate. This is caused by the low mobility and low diffusivity of ions. The bulk velocity along the flame line direction is almost zero near the work surface, so the bulk velocity contributes insignificantly, based on equations 11 and 12.

The ion and electron current density is shown separately in figures 13 and 14, respectively.

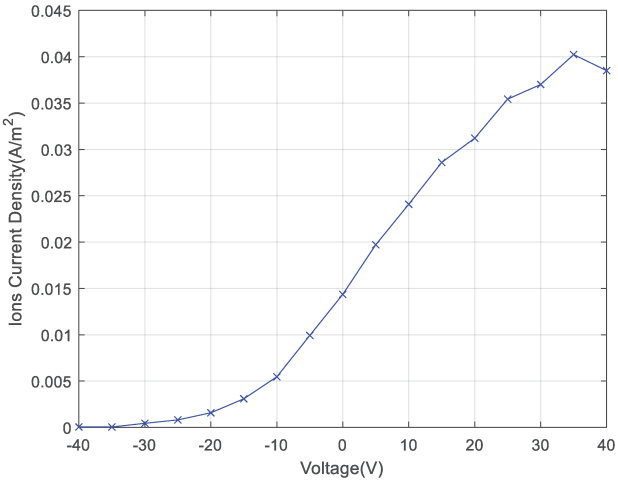

FIGURE 13: Ions current density at the center flame line above a work surface with different voltage.

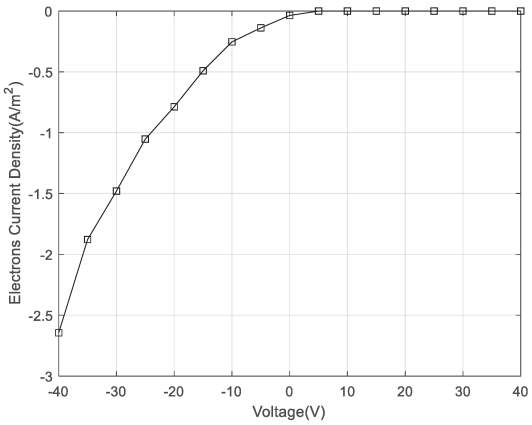

FIGURE 14: Electron current density at the center flame line above the work surface with different voltage.

One can see that the ion current density is saturated at high negative electric potentials, while electron current density is saturated in the positive electric potential region. The combination of both ion and electron density gives the electric current density. Thus, the electric characteristics can be analyzed from each figure. Based on the trend lines in figures 13 and 14, three different regimes can be identified. *Regime 1* is around -40V to -10V, where the ions current density is saturated, and the electron current density is following the Ohm's law. *Regime 2* is around -10 to 0V where both the ions and electron current density are following Ohm's law. *Regime 3* is around 0V to 35V where the ions current density obeys Ohm's law while the electron current density is saturated.

3.4 Comparison between 2D simulation and experiment

The 2D-model results are compared with the laboratory experiment data [1]. Figure 15 shows the test results reported by Martin et al.

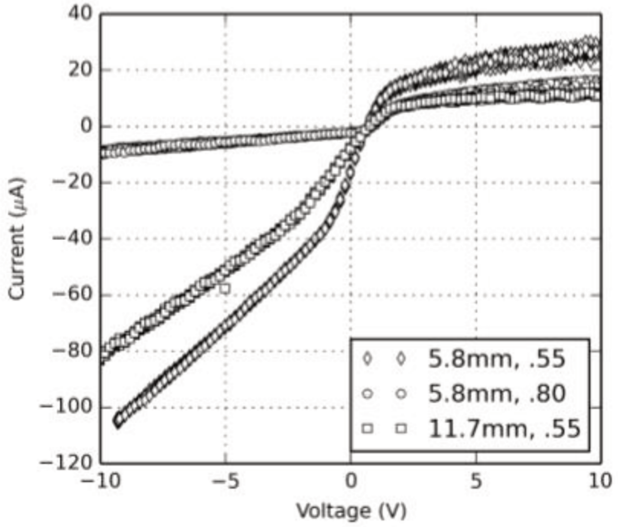

FIGURE 15: Current-voltage characteristics-experiment data for three different conditions [1].

In the figure, the three different conditions are based on the combination of different standoff and F/O ratios. Since the initial conditions and boundary conditions used in the simulations are slightly different in terms of some parameters, such as inlet velocity and standoff, only a qualitative comparison is applied here. First, the maximum value of positive current and negative current is around four times higher than the positive current shown in figure 15. At the same time, in the 2D-model results, the differences can be as high as fifty times the magnitude in both figures 13 and 14. The potential reasons can be as follows:

(1) the initial velocity prescribed at the inlet as a boundary condition is higher in the physical experiment
(2) the value for the mobility of ions should be larger than values used in the computational model, or
(3) since we only analyze the current density at the center flame line above the work surface, the distribution of the magnitude might be different between electrons and ions, considering a large radial velocity is observed along the whole work surface.

To further investigate the third reason listed above, the electron and ion current density at the work surface along the axial direction is shown in figure 16 and figure 17.

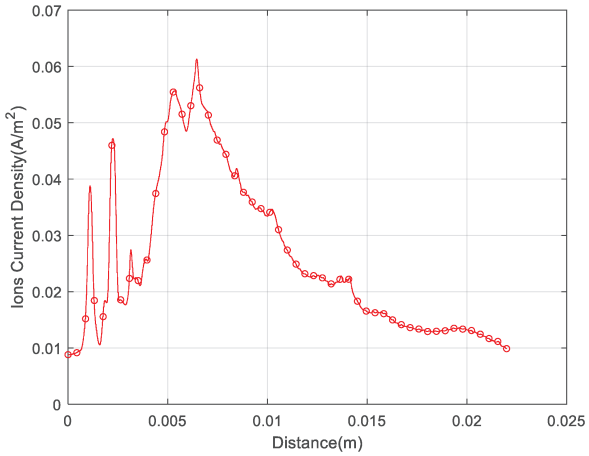

FIGURE 16: Ions current density among axial direction at the work surface at 40V condition.

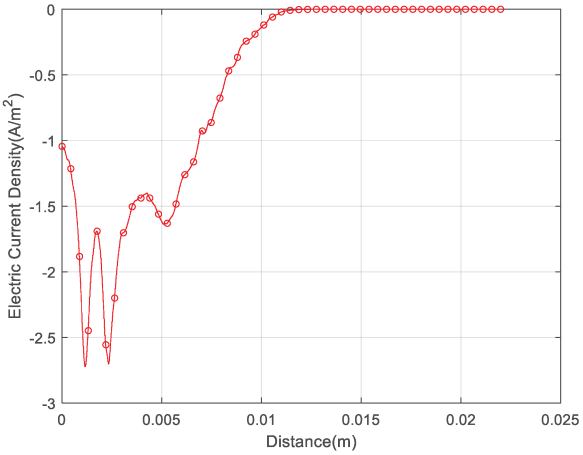

FIGURE 17: Electrons current density among axial direction at the work surface at -40V condition.

The ions current density is studied at the 40V case and electron current density is analyzed at the -40V case because the magnitude of current density is high in each case. The work surface has a 0.022m radial distance. One can see the ion current density always has a magnitude greater than 0.01 Am^{-2} along the entire surface, while the electron current density goes to zero when the radial distance is above 0.01m. The current can be calculated by integrating both the ion current density and electron current density over the work surface, which is considered a circle. The current-voltage characteristics calculated from the models are shown in figure 18.

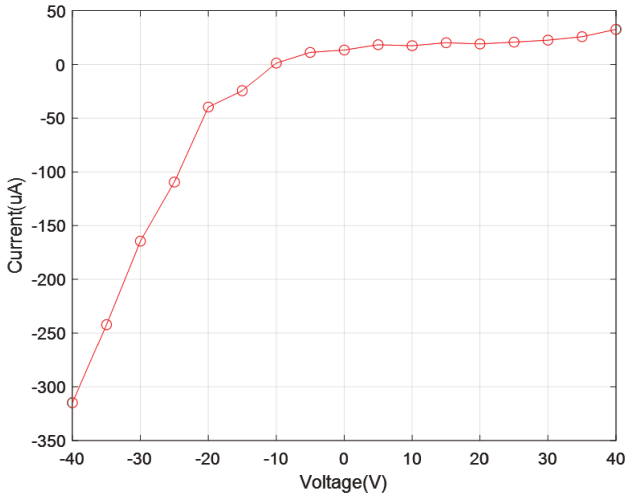

FIGURE 18: Current-voltage characteristics of the model.

From this figure, the three regimes can be identified clearly in different voltage ranges. When compared to figure 15, one can see the differences between modeling and the laboratory experiment. First to note is the magnitude differences. The negative currents seem to have larger magnitudes compared to the experiment when in high negative voltage conditions. Additionally, the current near 0V is negative in the experiment, while the model suggests it is positive. The voltage range considered in the experiment is smaller which means the current is more sensitive to voltage as well. The model has the largest standoff and F/O ratio compared to those three conditions. The larger the two parameters become, the less sensitive the current is to voltage. Therefore, the model's current change is slower with the same amount of voltage change compared to the experiment. As indicated by the experiment data, there is a positive current saturation region. In the 40V case of figure 13, the ion current density starts to remain close to the previous results, so there might be positive saturation for the ion current density when the voltage is higher.

4. CONCLUSION

A two-dimensional model is developed to analyze the transportation of electrons and ions inside a methane-oxygen flame flow. The transportation results illustrate the current-voltage characteristic and were compared to data from a laboratory experiment. The results show the current is increasing with the increasing voltage. In the positive regime, the increase is slow, while in the negative regime, the increase is rapid. Three different regimes are shown in the current-voltage relation caused by the saturation phenomena of both electron and ion current densities.

The differences between simulation results and test data are believed to be caused by neglecting the absorption and surface reactions. This hypothesis is planned to be tested in the follow-up work. Furthermore, in the experiments we discussed, the physical flame was comprised of twelve individual Bunsen-like conical flames. By neglecting the 3rd dimension, we have sacrificed the resolution of fluid mechanics and the interaction among the individual cones, but with a substantial simplification of the model as a cost.

ACKNOWLEDGEMENTS

This material is based upon work supported by the National Science Foundation under Grant No. 1900540.

REFERENCES

[1] Martin, C., Leonard, C., and VonFricken, J., 2017, "A study of the electrical characteristics of an oxy-fuel flame," Exp Therm Fluid Sci, 88, pp. 65-72.
[2] Belhi, M., Lee, B. J., Cha, M. S., and Im, H. G., 2019, "Three-dimensional simulation of ionic wind in a laminar premixed Bunsen flame subjected to a transverse DC electric field," Combust Flame, 202, pp. 90-106.
[3] Speelman, N., de Goey, L. P. H., and van Oijen, J. A., 2015, "Development of a numerical model for the electric current in burner-stabilised methane-air flames," Combust Theor Model, 19(2), pp. 159-187.
[4] Xiong, Y., Park, D. G., Lee, B. J., Chung, S. H., and Cha, M. S., 2016, "DC field response of one-dimensional flames using an ionized layer model," Combust Flame, 163, pp. 317-325.
[5] Martin, C., Untaroiu, A., and Xu, K., 2020, "A one dimensional model for ion transport in flame with two absorbing surfaces." Combustion Theory and Modelling, [Submitted].
[6] Yamashita, K., Karnani, S., and Dunn-Rankin, D., 2009, "Numerical prediction of ion current from a small methane jet flame," Combust Flame, 156(6), pp. 1227-1233.
[7] Martin, C. R., 2018, "A study of ion currents in an oxyfuel flame due to work surface chemical action," Exp Therm Fluid Sci, 98, pp. 239-250.
[8] "STAR CCM+ Users Manual," http://www.cd-adapco.com/products/star-ccm/documentation.
[9] Smith, G. P., Golden, D. M., Frenklach, M., Moriarty, N. W., Eiteneer, B., Goldenberg, M., Bowman, C. T., Hanson, R. K., Song, S., Gardiner, W. C., Jr., V. V. L., and Qin, Z., 1999, "http://www.me.berkeley.edu/gri_mech/."
[10] Belhi, M., Domingo, P., and Vervisch, P., 2010, "Direct numerical simulation of the effect of an electric field on flame stability," Combust Flame, 157(12), pp. 2286-2297.
[11] Chen, B. J., Wang, H. Y., Wang, Z. D., Han, J., Alquaity, A. B. S., Wang, H., Hansen, N., and Sarathy, S. M., 2019, "Ion chemistry in premixed rich methane flames," Combust Flame, 202, pp. 208-218.
[12] Martin, C., Untaroiu, A., and Xu, K., 2020, "Spatially resolved ion density measurements in an oxyfuel cutting flame." Combustion Science and Techonlogy, doi:10.1080/00102202.2020.1792458